

## Modification of thermal transport in few-layer MoS<sub>2</sub> by atomic-level defects engineering

*Yunshan Zhao<sup>1, ‡, \*</sup>, Minrui Zheng<sup>2, ‡</sup>, Jing Wu<sup>3</sup>, Xin Guan<sup>4</sup>, Ady Suwardi<sup>3</sup>, Yida Li<sup>5</sup>, Manohar Lal<sup>2</sup>, Guofeng Xie<sup>6</sup>, Gang Zhang<sup>7, \*</sup>, Lifa Zhang<sup>1, \*</sup>, John T L Thong<sup>2, \*</sup>*

<sup>1</sup>NNU-SULI Thermal Energy Research Center (NSTER) & Center for Quantum Transport and Thermal Energy Science (CQTES), School of Physics and Technology, Nanjing Normal University, Nanjing, 210023, China

<sup>2</sup>Department of Electrical and Computer Engineering, National University of Singapore, 117583, Singapore

<sup>3</sup>Institute of Materials Research and Engineering, Agency for Science, Technology and Research, 138634, Singapore

<sup>4</sup>International Studies College, National University of Defense Technology, Nan Jing, 210012, China

<sup>5</sup>Engineering Research Center of Integrated Circuits for Next-Generation Communications, Ministry of Education, Southern University of Science and Technology, Shenzhen 518055, China

<sup>6</sup>Hunan University of Science and Technology, Xiangtan, 411201, China

<sup>7</sup>Institute of High Performance Computing, Agency for Science, Technology and Research, 138632, Singapore

<sup>‡</sup> These authors contributed equally to this work.

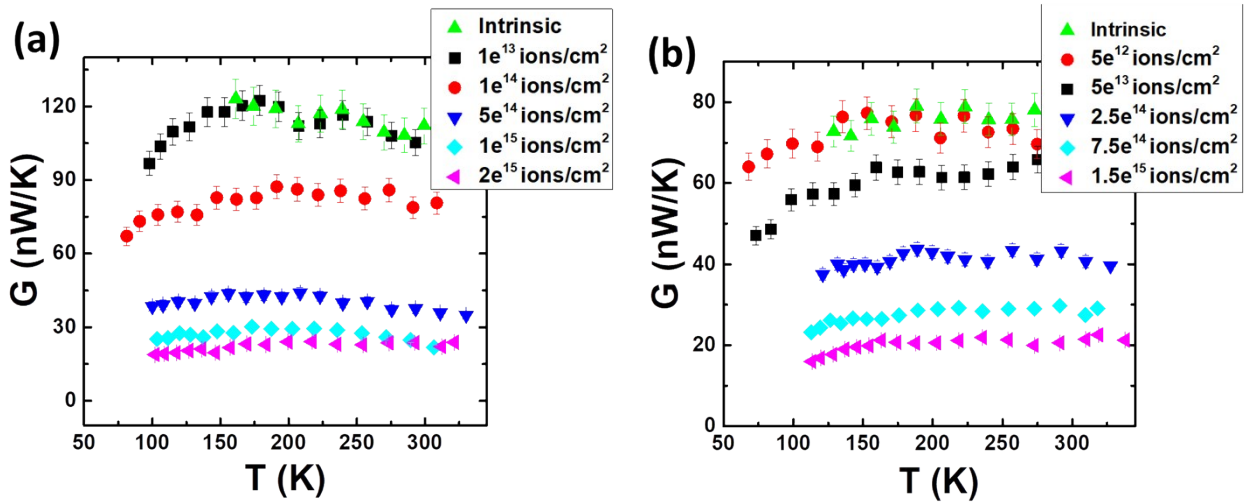


Figure S1 Thermal transport characterization of two MoS<sub>2</sub> flakes (a) and (b) as a function of temperature. The irradiation doses are illustrated on each figure.

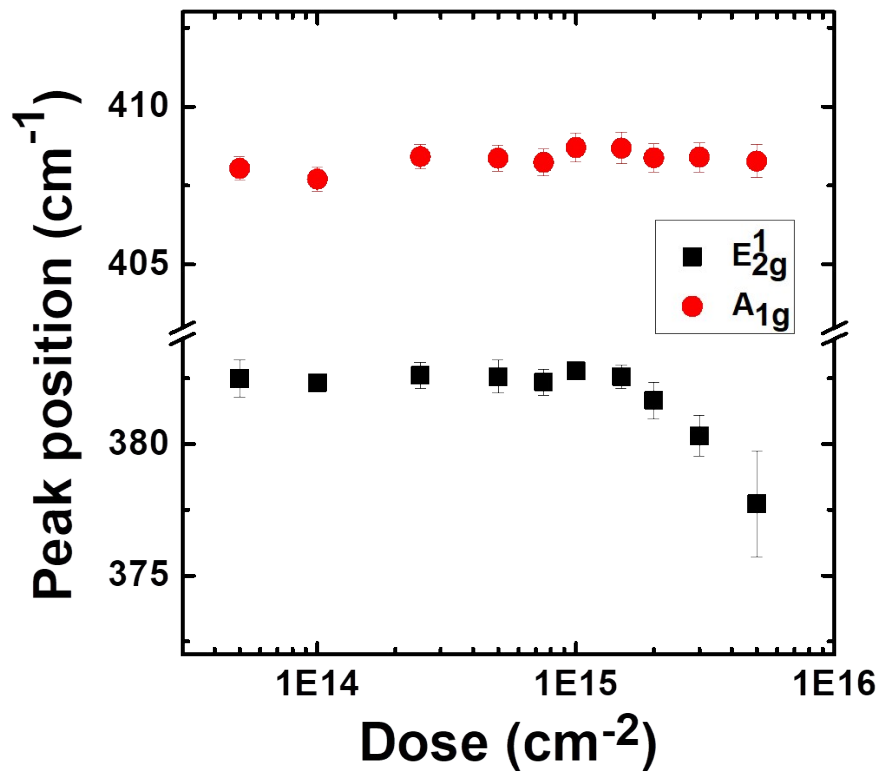


Figure S2 Raman characterization of defected MoS<sub>2</sub> flakes. In-plane E<sub>2g</sub><sup>1</sup> peak shows a red-shift while out-of-plane A<sub>1g</sub> shows a slight blue-shift with increasing the dose.

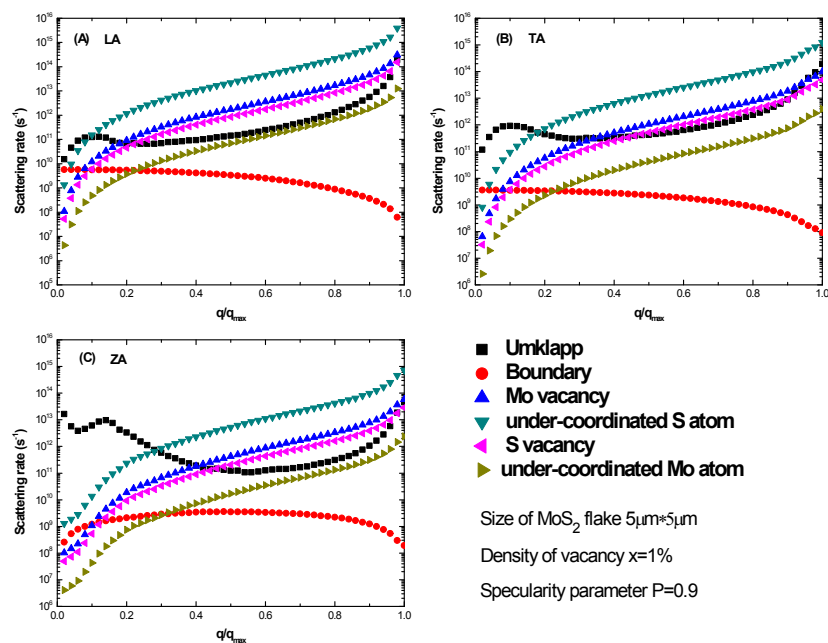


Figure S3 Various scattering rates of LA phonons (a), TA phonons (b) and ZA phonons (c) as functions of normalized wave vector at room temperature.

## Supporting Information 1 Transferring few-layer MoS<sub>2</sub> onto fully suspended pads

Prior to the transfer of thin MoS<sub>2</sub> flakes onto fully-suspended pads, few-layer MoS<sub>2</sub> flakes were mechanically exfoliated from a bulk piece of MoS<sub>2</sub> (HQ Graphene) onto a Si wafer with 285 nm SiO<sub>2</sub> overlayer. The wafer surface was cleaned by soaking in acetone overnight and subsequently rinsed in IPA and blown dry to get rid of tape residues. A thin layer (~180 nm) of a relatively low molecular weight (495k) PMMA was spin-coated on the wafer and baked at 180 °C for 2 min. A supporting tape (Nitto ELP BT-150E-KL) with a 5 mm punctured hole was pasted onto the PMMA layer, such that the target flake to be transferred appeared approximately at the hole center. The entire wafer assembly with the PMMA layer and supporting tape was floated on a 15% KOH solution until the SiO<sub>2</sub> layer was completely etched and the Si wafer sunk to bottom of beaker. The supporting tape, now loaded with the PMMA layer and target flake, was carefully rinsed in DI water a few times and dried.

The supporting film was then mounted onto a mechanical arm connected to a manual XYZ stage, and the wafer containing the fully-suspended METS device was attached to a heating stage. The supporting film was lowered carefully under an optical microscope (Leica DM100, 50X objective lens) until the target flake settled into the region between the suspended pads. At this moment, a gentle heating (typically up to 100 °C) was applied to the METS substrate such that the PMMA film could stick very firmly to the substrate. It was then torn off from the supporting tape around the 5 mm hole edge.

The METS device was subsequently soaked in acetone overnight to remove the PMMA layer, and transferred to a critical point dryer (Leica EM CPD300) with a selection of most gentle drying process (typically up to 3 hours per run) to fully dry the sample with high levels of cleanliness, while preserving fully-suspended sample geometry. The overall success yield of the transfer process achieved is about 20%. It should be pointed out that for the transfer of CVD-grown monolayer MoS<sub>2</sub> flakes onto a TEM grid for HIM irradiation and STEM imaging, we followed the same general transfer procedure, with the exception of not using a supporting film and the entire alignment procedure while lowering the target flake. In this case, the TEM grid was simply held to scoop up the PMMA layer (laden with CVD-grown monolayer MoS<sub>2</sub> flakes) floating on DI water.

In the measured thermal conductivity, we assume that two parts of the measured flake are connected in parallel. Thus, for the sample with two different contact areas in the two ends,  $\kappa$  is got by  $\kappa = \kappa_1 + \kappa_2 \frac{G_1 \times L_1}{S_1} + \frac{G_2 \times L_2}{S_2}$ ; for the sample with same contact areas in the two ends, the thermal conductivity value can be obtained by  $\kappa = G \times L / S$ . Therefore, the fluctuation and errors come from the uncertainty in measuring the area, by measuring the width and length under SEM and measuring the thickness by AFM before transferring the flake on top of METS. We did one measurement for three times and then took average.

## **Supporting Information 2 He<sup>+</sup> ion irradiation on MoS<sub>2</sub> flake for STEM characterization**

In order to apply the atomic-scale imaging technique using aberration-corrected scanning transmission electron microscopy (AC-STEM) to reveal the detailed point defect generation process in MoS<sub>2</sub> flakes and its dependence on irradiating He<sup>+</sup> ion doses, we have chosen CVD-grown monolayer MoS<sub>2</sub> flakes as a model system for this part of the study.

Triangular CVD-grown monolayer MoS<sub>2</sub> flakes on Si wafers with a 285 nm SiO<sub>2</sub> overlayer were purchased from SixCarbon Technology (Shenzhen) Ltd. The flakes were transferred onto a 400 mesh Cu TEM finder grid covered with lacey carbon support film using a PMMA-assisted wet transfer approach and dried using a critical point dryer. Exact locations of suspended triangular monolayer MoS<sub>2</sub> flakes were identified using optical microscopy.

The TEM grid was subsequently loaded into a Zeiss Orion Nanofab helium ion microscope (HIM) for He<sup>+</sup> ion irradiation. The portions of the flakes over the lacey carbon support were confirmed *in situ* using a quick HIM imaging mode, and squares with 10  $\mu$ m side lengths as typical irradiation patterns were drawn for this study. We fixed the pixel spacing as 2 nm across all irradiation patterns, and by varying the dwell time per pixel across different irradiation patterns, the total areal irradiation dose was varied systematically in the range between  $1 \times 10^{12}$  ions/cm<sup>2</sup> to  $1 \times 10^{16}$  ions/cm<sup>2</sup>. To get low dose, we can reduce the current during irradiation, as well as increase the irradiation area, as  $dose = I \times t / eA$ , where I is the beam current, t is the irradiation time, e is the electron charge and A is the irradiation area.

## **Supporting Information 3 First-principles calculation for phonon scattering rate**

The Matthiessen's rule is applied to combine the different phonon scattering mechanisms, therefore

$$\tau_{\lambda}^{-1} = \tau_{U,\lambda}^{-1} + \tau_{B,\lambda}^{-1} + \tau_{V,\lambda}^{-1} + \tau_{A,\lambda}^{-1} \quad (1)$$

where  $\tau_{U,\lambda}^{-1}$  is the Umklapp phonon-phonon scattering rate,  $\tau_{B,\lambda}^{-1}$  is the phonon-boundary scattering rate,  $\tau_{V,\lambda}^{-1}$  is the phonon-vacancy scattering rate, and  $\tau_{A,\lambda}^{-1}$  is the scattering rate of phonons by the under-coordinated atoms near the vacancies. The expression and its parameters of  $\tau_{U,\lambda}^{-1}$  and  $\tau_{B,\lambda}^{-1}$  are the same as our previous work<sup>1</sup>.  $\tau_{V,\lambda}^{-1}$  is derived from Klemen's perturbation theory in terms of the missing mass and the missing linkages<sup>2</sup>,

$$\tau_{V,\lambda}^{-1} = x \left( \frac{\Delta M}{M} \right)^2 \frac{\pi \omega^2 g(\omega)}{2 G} \quad (2)$$

where  $x$  is the density of vacancy,  $G$  is the number of atoms in the crystal,  $g(\omega)$  is the phonon density of states (DOS). For vacancy defect, the effective value of  $\frac{\Delta M}{M}$  is  $-\frac{M_a}{M} - 2$ , where  $M$  is the average mass per atom,  $M_a$  is the mass of the missing atom.

In our previous work, we found the phonon scattering mechanism by the under-coordinated atoms near the vacancies and derived the scattering rate as<sup>3</sup>,

$$\tau_{A,\lambda}^{-1} = 4\pi x_A \left\{ \left[ \frac{1 + \exp[(12-z)/(8z)]}{1 + \exp[(13-z)/(8z-8)]} \right]^{-(m+2)} - 1 \right\}^2 \frac{\omega^2 g(\omega)}{G} \quad (3)$$

where  $x_A$  is the density of the under-coordinated atoms,  $z$  is the effective coordination number, and  $m$  is a key parameter that represents the nature of the bond ( $m=4$  for MoS<sub>2</sub>). In MoS<sub>2</sub>, the coordination number of Mo and S atom is 6 and 3 respectively. Around a Mo vacancy, there are six under-coordinated S atoms whose coordination number is changed from 3 to 2, and around a S vacancy, there are three under-coordinated Mo atoms whose coordination number is changed from 6 to 5.

## References

1. Wei, X.; Wang, Y.; Shen, Y.; Xie, G.; Xiao, H.; Zhong, J.; Zhang, G. *Applied Physics Letters* **2014**, 105, (10), 103902.
2. Ratsifaritana, C.; Klemens, P. *International journal of thermophysics* **1987**, 8, (6), 737-750.
3. Xie, G.; Shen, Y.; Wei, X.; Yang, L.; Xiao, H.; Zhong, J.; Zhang, G. *Scientific reports* **2014**, 4, 5085.